

Full-Duplex Massive MIMO Cellular Networks with Low Resolution ADC/DAC

Elyes Balti and Brian L. Evans

Wireless Networking and Communications Group
The University of Texas at Austin, Austin, TX, USA
ebalti@utexas.edu, bevans@ece.utexas.edu

Abstract—In this paper, we provide an analytical framework for full-duplex (FD) massive multiple-input multiple-output (MIMO) cellular networks with low resolution analog-to-digital and digital-to-analog converters (ADCs and DACs). Matched filters are employed at the FD base stations (BSs) at the transmit and receive sides. For both reverse and forward links, we derive the expressions of the signal-to-quantization-plus-interference-and-noise ratio (SQINR) for general and special cases. We further evaluate the outage probability and spectral efficiency for reverse and forward links, and quantify the effects of the quantization error, loopback self-interference and inter-user interference for cells arranged in a hexagonal lattice and Poisson Point Process (PPP) tessellations. Finally, we derive analytical expressions for spectral efficiency for asymptotic cases as well as for power scaling laws.

Index Terms—Full Duplex, Massive MIMO, Low Resolution Data Converters, Cellular Networks, Interference.

I. INTRODUCTION

Full duplex (FD) has emerged as an attractive solution to double the spectral efficiency because the transmission and the reception occur simultaneously in the same resource blocks. In addition, FD devices can use a shared array, i.e., the same array can be used for transmission and reception without dedicating two separate arrays, which can substantially reduce cost. These benefits make FD applicable in practice such as machine-to-machine and integrated access and backhaul which is currently proposed in 3GPP release 17 [1]. Although FD brings many advantages, it suffers from loopback self-interference (SI) caused by the simultaneous transmission and reception in the same resource blocks. This loopback signal cannot be neglected as the relative SI power can be several orders or magnitude stronger than the received signal power, which can render FD systems dysfunctional [2], [3].

To overcome this limitation, massive MIMO has been proposed as a viable solution to enable FD operation. A massive number of antennas can provide enough degrees of freedom (DoF) not only to improve the spatial multiplexing gain but also substantially mitigate the SI. Thanks to these benefits, massive MIMO FD has been considered for cellular networks, millimeter wave applications such as IEEE 802.11ad and 802.11ay Wi-Fi standards, and 5G New Radio (NR) in 3GPP Release 15 [4]–[6].

Employing a massive number of antennas, however, can lead to huge power consumption, particularly for full-digital systems wherein each RF chain and ADC/DAC are dedicated

for each antenna element. In addition, this power consumption can be prohibitive for the higher bandwidths in millimeter wave applications. For this reason, several researchers have proposed low-resolution ADCs/DACs to reduce the power consumption at the expense of spectral efficiency [7]. Increasingly, energy efficiency is becoming a more important system design measure than spectral efficiency.

In this context, we consider the application of FD with low resolution ADCs and DACs in cellular networks. The BS operates in FD mode while the user equipments (UEs) are operating in half-duplex mode. Due to the limited space, we defer the analysis of pilot contamination in an extension of this work, and for now, assume pilot orthogonality is maintained across the network cells. The results are simulated for a hexagonal lattice with different tiers as well as Voronoi tessellation for Poisson Point Process (PPP) networks. To the best of our knowledge, this is the first work which considers the application of FD systems with low resolution ADCs and DACs for cellular networks.

The remainder of this paper is organized as follows: Section II discusses the network model, while analyses of the reverse and forward links are provided by Sections III and IV, respectively. Asymptotic analysis and power scaling laws are derived in Section V, and numerical results are reported in Section VI. Concluding remarks appear in Section VII.

For notation, italic non-bold letter refers to a scalar while bold lower case and bold upper case stand for vector and matrix, respectively. We further denote the scripting u and d for uplink and downlink, respectively.

II. NETWORK MODEL

We consider a macrocellular network where each BS operates in FD mode and is equipped with $N_a \gg 1$ antennas. Each UE operates in half-duplex mode and has a single antenna.

A. Large-Scale Fading

Each UE is associated with the BS from which it has the strongest large-scale channel gain and we denote by K_ℓ^u and K_ℓ^d the number of uplink and downlink UEs served by the ℓ -th BS. The large-scale gain comprises pathloss with exponent $\eta > 2$ and shadowing that is independently and identically distributed (IID) across the paths. In particular, the large-scale

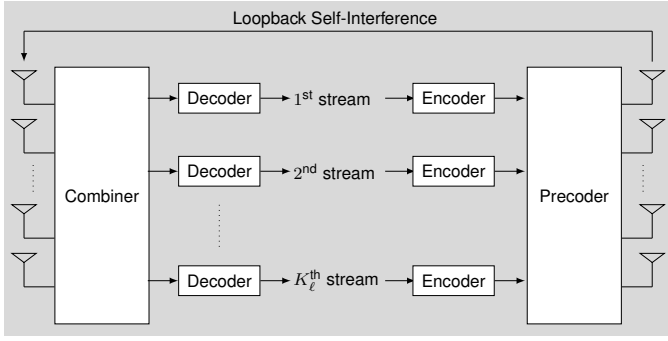


Fig. 1: Basic abstraction of a full-duplex base station: The uplink user equipment (UE) sends the data to the base station (BS) independently from the data intended to the downlink UE sent from the BS. Since the BS transmits and receives simultaneously in the same resource blocks, SI leakage is created in the form of a loopback from TX to RX sides of the BS.

gain between the ℓ -th BS and the k -th user connected to the l -th BS is

$$G_{\ell,(l,k)} = \frac{L_{\text{ref}}}{r_{\ell,(l,k)}^\eta} \chi_{\ell,(l,k)} \quad (1)$$

with L_{ref} as the pathloss intercept at a unit distance, $r_{\ell,(l,k)}$ the link distance, and $\chi_{\ell,(l,k)}$ as the shadowing coefficient satisfying $\mathbb{E}[\chi^\delta] < \infty$, where $\delta = 2/\eta$.

Without loss of generality, we denote the 0-th BS as the focus of interest and we drop its subscript.

Further, we introduce large-scale fading between the UEs to model the inter-user communication. We denote $T_{(\ell,n),(l,k)}$ as the large-scale channel gain between the n -th user and the k -th user associated with the ℓ -th and l -th BSs, respectively.

B. Small-Scale Fading

We denote $\mathbf{h}_{\ell,(l,k)} \sim \mathcal{N}_{\mathbb{C}}(\mathbf{0}, \mathbf{I})$ as the normalized reverse link $N_a \times 1$ small-scale fading between the k -th user located in cell l and the BS in cell ℓ and $\mathbf{h}_{\ell,(l,k)}^*$ as the forward link reciprocal, assuming time division duplexing (TDD) with perfect calibration. In addition, we denote by $\mathbf{g}^{(\ell,n),(l,k)} \sim \mathcal{N}_{\mathbb{C}}(0, \sigma_{\text{fui}}^2)$ the 1×1 small-scale fading between the n -th user in cell ℓ and the k -th user in cell l . We further denote by $\mathbf{H}_{\text{SI}} \sim \mathcal{N}_{\mathbb{C}}(\mathbf{0}, \boldsymbol{\mu}_{\text{SI}}^2)$ the SI channel matrix ($N_a \times N_a$).

Remark. In this work, we assume perfect knowledge of the SI channel. This assumption can be adopted since the line-of-sight (LOS) component (near-field) of the SI channel is dominant and deterministic while the external non-LOS SI channel component is random and negligible. Without loss of generality, we consider a random SI channel matrix. The estimation of the SI channel can be carried out with conventional methods such as Least Square (LS) or Minimum Mean Square Error (MMSE) estimators. If the channel matrix is sparse, then the compressive sensing method will be the best candidate, in particular, for large matrix dimension. In addition, we can still consider an estimate of the SI channel ($\hat{\mathbf{H}}_{\text{SI}}$) while the estimation error can be accounted as additional source of SI. Note that tackling the SI channel estimation problem is out of the scope of this work.

C. Quantized Signal Model

For infinite resolution, a typical received signal \mathbf{y} is

$$\mathbf{y} = \mathbf{H}\mathbf{x} + \mathbf{n} \quad (2)$$

where \mathbf{H} , \mathbf{x} , and \mathbf{n} are the channel matrix, the precoded symbols and the additive white Gaussian noise (AWGN), respectively. Several nonlinear quantization models have been proposed in the literature; however, the analysis of such models is complex for a higher number of ADC bits. In quantized systems, a lower bound to the spectral efficiency has been derived by treating the quantization as additive Gaussian noise with variance inversely proportional to the resolution of the quantizer, i.e. 2^{-b} times the received input power where b is the number of ADC bits. Recent publications [8], [9] have considered the additive quantization noise model (AQNM) for mmWave signals with an arbitrary number of ADC bits. In addition, the work [10] derived Gaussian approximations using Bussgang Theory to linearize the nonlinear quantization distortion which is quite similar to the AQNM. The received signal (2) is processed through the RF chains and then converted to the digital discrete-time domain by the ADC. The AQNM represents the quantized version of (2) given by

$$\mathbf{y}_q = \alpha\mathbf{y} + \mathbf{q} \quad (3)$$

where \mathbf{q} is the additive quantization noise, $\alpha = 1 - \rho$ and ρ is the inverse of the signal-to-quantization-plus-noise ratio (SQNR), which is inversely proportional to the square of the resolution of an ADC, i.e., $\rho = \frac{\pi\sqrt{3}}{2} \cdot 2^{-2b}$.

TABLE I: ρ for different values of b ($b \leq 5$) [10].

b	1	2	3	4	5
ρ	0.3634	0.1175	0.03454	0.009497	0.002499

III. REVERSE LINK ANALYSIS

The k -th uplink user in cell ℓ sends the data symbol $s_{\ell,k} \sim \mathcal{N}_{\mathbb{C}}(0, 1)$. Since the BS operates in FD mode, the signal intended to downlink users is leaked to the receive array of the BS and incurs loopback SI that corrupts the uplink users. Upon data transmission from the users, the BS of interest observes the following quantized received signal vector

$$\begin{aligned} \mathbf{y}^u = & \alpha_u \sum_{\ell} \sum_{k=0}^{K_{\ell}^u - 1} \sqrt{G_{\ell,k} P_{\ell,k}} \mathbf{h}_{\ell,k} s_{\ell,k} + \alpha_u \sqrt{P_{\text{SI}}} \mathbf{H}_{\text{SI}} \mathbf{q}_d \\ & + \alpha_u \alpha_d \sqrt{P_{\text{SI}}} \sum_{k=0}^{K^d - 1} \mathbf{H}_{\text{SI}} \mathbf{f}_k s_k^d + \mathbf{q}_u + \alpha_u \mathbf{v} \end{aligned} \quad (4)$$

where $P_{\ell,k}$ is the transmit power of the uplink user served by the BS of interest to the ℓ -th BS and $\mathbf{v} \sim \mathcal{N}_{\mathbb{C}}(\mathbf{0}, \mathbf{I})$ is the additive white Gaussian noise (AWGN) vector ($N_a \times 1$).

A. Channel Hardening

One of the benefits of having a massive number of antennas is the hardening of the filtered signals. Suppose that, rather than $\mathbf{w}_k^* \hat{\mathbf{h}}_k$ ($\hat{\mathbf{h}}$ is the estimate of \mathbf{h}), the decoder regards $\mathbb{E}[\mathbf{w}_k^* \mathbf{h}_k]$ as the filtered channel. The receiver can compute

this value from the channel statistics while the fluctuation of the filtered signal around the mean can be treated as self-interference. By decomposing the interference into inter-cell and intra-cell and applying the linear receive filter \mathbf{w}_k^* at the k -th user ($y_k = \mathbf{w}_k^* \mathbf{y}$), the received signal at the BS of interest of the k -th user is given by (5) on the next page.

B. Matched Filter Receiver

We adopt the matched filter receiver to design the combiner \mathbf{w}_k , $k = 0, \dots, K^u - 1$.

Corollary 1. *The matched filter receiver \mathbf{w}_k^{MF} (transmitter \mathbf{f}_k^{MF}) has the following properties*

- 1) $\mathbb{E} [\|\mathbf{w}_k^{\text{MF}}\|^2] = \mathbb{E} [\|\mathbf{f}_k^{\text{MF}}\|^2] = N_a$.
- 2) $\mathbb{E} [\|\mathbf{w}_k^{\text{MF}}\|^4] = \mathbb{E} [\|\mathbf{f}_k^{\text{MF}}\|^4] = N_a^2 + N_a$.
- 3) $\mathbb{E} [|\mathbf{w}_k^{\text{MF}*} \mathbf{h}_{\ell,k}|^2] = \mathbb{E} [|\mathbf{h}_{\ell,k}^* \mathbf{f}_{\ell,k}^{\text{MF}}|^2] = N_a$.

Theorem 1. *The output SQINR of the k -th uplink user is (6).*

$$\overline{\text{sqinr}}_k^{\text{MF}} = \frac{\alpha_u^2 G_k P_k |\mathbb{E}[\mathbf{w}_k^{\text{MF}*} \mathbf{h}_k]|^2}{\overline{\text{den}}_u^{\text{MF}}} \quad (6)$$

where $\overline{\text{den}}_u^{\text{MF}}$ is given by (7) on the next page.

The numerator of (6) and the first four terms of (7) on the next page can be solved using the properties in Corollary 1, while the remaining terms of (7) can be derived as follows

$$\sum_{k=0}^{K^d-1} \mathbb{E} [|\mathbf{w}_k^* \mathbf{H}_{\text{SI}} \mathbf{f}_k|^2] = \mu_{\text{SI}}^2 K^d N_a^2 \quad (8)$$

$$\mathbb{E} [|\mathbf{w}_k^* \mathbf{H}_{\text{SI}} \mathbf{q}_d|^2] = \alpha_d (1 - \alpha_d) \mu_{\text{SI}}^2 N_a^2 \quad (9)$$

$$\mathbb{E} [|\mathbf{w}_k^* \mathbf{q}_u|^2] = N_a \alpha_u (1 - \alpha_u) \left[2G_k P_k + \sum_{k \neq k} G_k P_k + \sum_{\ell \neq 0} \sum_k G_{\ell,k} P_{\ell,k} + \alpha_d P_{\text{SI}} \mu_{\text{SI}}^2 N_a + \sigma^2 \right] \quad (10)$$

Proof. The proof of (8), (9), and (10) are provided by Appendix A in [7]. \square

With $\overline{\text{sqinr}}_k^{\text{MF}}$, $k = 0, \dots, K^u - 1$, stable over the respective local neighborhoods, the evaluation of the gross spectral efficiencies does not require averaging over the fading realizations, but rather is directly computed as

$$\frac{\bar{\mathcal{I}}_k}{B} = \log \left(1 + \overline{\text{sqinr}}_k \right), \quad k = 0, \dots, K^u - 1 \quad (11)$$

where B is the bandwidth.

Corollary 2. *To further characterize the spectral efficiency, we can derive a new bound using the following formula. Assuming statistical independence between x and y , we have*

$$\mathbb{E} \left[\log \left(1 + \frac{x}{y} \right) \right] \cong \log \left(1 + \frac{\mathbb{E}[x]}{\mathbb{E}[y]} \right) \quad (12)$$

Assuming perfect channel state information (CSI), i.e., without channel hardening, and applying Corollary 2, the numerator of (6) becomes

$$\overline{\text{num}}_u^{\text{MF}} = \alpha_u^2 G_k P_k \mathbb{E} \left[|\mathbf{w}_k^{\text{MF}*} \mathbf{h}_k|^2 \right] = \alpha_u^2 G_k P_k (N_a^2 + N_a) \quad (13)$$

while the first term of (7) vanishes since the CSI is perfect.

Proposition 1. *Considering a single-cell multiuser system (without any inter-cell interference) with perfect CSI, Corollary 2 entails the results for uplink users in [7].*

IV. FORWARD LINK ANALYSIS

The signal transmitted by the ℓ -th BS is

$$\mathbf{x}_\ell = \sum_{k=0}^{K_\ell^d-1} \sqrt{\frac{P_{\ell,k}}{N_a}} \mathbf{f}_{\ell,k} s_{\ell,k} \quad (14)$$

where $P_{\ell,k}$ is the power allocated to the data symbol $s_{\ell,k} \sim \mathcal{N}_{\mathbb{C}}(0, 1)$, which is precoded by $\mathbf{f}_{\ell,k}$ and intended for its k -th user. The power allocation satisfies

$$\sum_{k=0}^{K_\ell^d-1} P_{\ell,k} = P \quad (15)$$

where P is the downlink power per cell. Since the BS operates in FD mode, the uplink users are only corrupted by the SI while the downlink users are SI-free. But since the uplink users are sending simultaneously when the downlink users are receiving, the latter are vulnerable to the inter-user interference caused by the uplink users.

Upon data transmission from the BS of interest, the k -th user observes the following quantized received signal from the BS of interest as

$$\begin{aligned} y_k^d = & \alpha_d \sum_{\ell} \sum_{k=0}^{K_\ell^d-1} \sqrt{\frac{G_{\ell,k} P_{\ell,k}}{N_a}} \mathbf{h}_{\ell,k}^* \mathbf{f}_{\ell,k} s_{\ell,k} \\ & + \sum_{\ell} \sum_{k=0}^{K_\ell^d-1} \sqrt{\frac{G_{\ell,k} P_{\ell,k}}{N_a}} \mathbf{h}_{\ell,k}^* \mathbf{q}_{d,\ell} \\ & + \sum_{\ell} \sum_{k=0}^{K_\ell^u-1} \sqrt{T_{(\ell,k),k} P_{\ell,k}^u} \mathbf{g}_{(\ell,k),k} s_{\ell,k}^u + v_k \end{aligned} \quad (16)$$

A. Channel Hardening

Since we consider receivers reliant on channel hardening, the k -th user served by the BS of interest regards $\mathbb{E}[\mathbf{h}_k^* \mathbf{f}_k]$ as its precoded channel wherein the small-scale fading is averaged. The variation of the actual precoded channel around the mean incurs self-interference, such that (16) can be formulated as (17).

B. Matched Filter Precoder

The ℓ -th BS gathers the channel estimates $\hat{\mathbf{h}}_{\ell,(\ell,0)}, \dots, \hat{\mathbf{h}}_{\ell,(\ell,K_\ell^d-1)}$ from the reverse link pilots

$$\begin{aligned} \overline{\text{den}}_d^{\text{MF}} = & \alpha_d^2 \frac{G_k P_k}{N_a} \text{var} \left[\mathbf{h}_k^* \mathbf{f}_k^{\text{MF}} \right] + \alpha_d^2 \sum_{k \neq k} \frac{G_k P_k}{N_a} \mathbb{E} \left[\left| \mathbf{h}_k^* \mathbf{f}_k^{\text{MF}} \right|^2 \right] + \alpha_d^2 \sum_{\ell \neq 0} \sum_{k=0}^{K_\ell^d - 1} \frac{G_{\ell,k} P_{\ell,k}}{N_a} \mathbb{E} \left[\left| \mathbf{h}_{\ell,k}^* \mathbf{f}_{\ell,k} \right|^2 \right] \\ & + \sum_{k \neq k} T_{k,k} P_k^u \mathbb{E} \left[\left| \mathbf{g}_{k,k} \right|^2 \right] + \sum_{\ell \neq 0} \sum_{k=0}^{K_\ell^d - 1} T_{(\ell,k),k} P_{\ell,k}^u \mathbb{E} \left[\left| \mathbf{g}_{(\ell,k),k} \right|^2 \right] + \sum_{\ell} \frac{G_{\ell,k} P_{\ell,k}}{N_a} \mathbb{E} \left[\left| \mathbf{h}_{\ell,k}^* \mathbf{q}_\ell \right|^2 \right] + \sigma^2 \end{aligned} \quad (20)$$

$$\frac{\bar{\mathcal{I}}_k^u}{B} \rightarrow \log \left(1 + \frac{G_k P_k N_a^2}{\sum_{\ell} \sum_k G_{\ell,k} P_{\ell,k} N_a + P_{\text{SI}} \mu_{\text{SI}}^2 K^d N_a^2 + \sigma^2} \right) \quad (24)$$

$$\frac{\bar{\mathcal{I}}_k^d}{B} \rightarrow \log \left(1 + \frac{G_k P_k}{\sum_{\ell} \sum_k G_{\ell,k} P_{\ell,k} + \sum_{\ell} \sum_k T_{(\ell,k),k} P_{\ell,k}^u \sigma_{\text{iui}}^2 + \sigma^2} \right) \quad (25)$$

From (24) and (25), the quantization error incurred by ADC/DAC is removed for full-resolution. When the number of antennas is fixed, the spectral efficiency for uplink/downlink users become constant. Although the increasing ADC/DAC resolution can enhance the performance, the rate is still limited.

Lemma 2. *For a fixed number of antennas, fixed b and when $P_{\text{SI}} = P^d = P^u \rightarrow \infty$, the spectral efficiency converges to*

$$\frac{\bar{\mathcal{I}}_k^u}{B} \rightarrow \log \left(1 + \frac{\alpha_u G_k N_a}{\sum_{\ell} \sum_k G_{\ell,k} + (1 - \alpha_u) G_k + \alpha_d N_a \mu_{\text{SI}}^2 [1 + \alpha_u \alpha_d (K^d - 1)]} \right) \quad (26)$$

$$\frac{\bar{\mathcal{I}}_k^d}{B} \rightarrow \log \left(1 + \frac{\alpha_d^2 G_k}{\alpha_d^2 \sum_{\ell} \sum_k G_{\ell,k} + \sum_{\ell} \sum_k T_{(\ell,k),k} \sigma_{\text{iui}}^2 + \alpha_d (1 - \alpha_d) \sum_{\ell} G_{\ell,k} (K_\ell^d + 1)} \right) \quad (27)$$

From (26) and (27), we observe that the uplink spectral efficiency relies on the number of antennas N_a as well as the number of quantization bits b when the transmit power of the BS and users go to infinity. We also note that the spectral efficiency is saturated by irreducible ceiling caused by the SI and the quantization error.

Lemma 3. *If the transmit powers of the BS and each user is scaled with the number of antennas N_a i.e., $P = \frac{E}{N_a}$ where E is fixed, as $N_a \rightarrow \infty$, the spectral efficiency converges to*

$$\frac{\bar{\mathcal{I}}_k^u}{B} \rightarrow \log \left(1 + \frac{\alpha_u G_k E_k}{\alpha_d \mu_{\text{SI}}^2 E_{\text{SI}} [1 + \alpha_u \alpha_d (K^d - 1)] + \sigma^2} \right) \quad (28)$$

We found that using a proper power scaling law and more antennas can eliminate the intra-cell and inter-cell interference.

The number of quantization bits provides an approximation of the uplink spectral efficiency when N_a goes to infinity.

$$\frac{\bar{\mathcal{I}}_k^d}{B} \rightarrow \log \left(1 + \frac{\alpha_d^2 G_k E_k}{\sigma^2} \right) \quad (29)$$

(29) implies that using a proper power scaling and more antennas can eliminate the inter-user interference caused by full-duplexing. The number of quantization bits determines the approximate downlink spectral efficiency when the number of the antennas at a FD BS, N_a , goes to infinity.

VI. NUMERICAL RESULTS

In this section, we provide the numerical results of the system performance along with the discussion. Unless otherwise stated, Table II presents the values of the system parameters. We assume uniform power allocation for the forward links.

Fig. 2 provides the results of the cumulative distribution function (CDF) or the outage probability of the downlink SQINR. The performance for PPP tessellation serve as an upper bound for the hexagonal lattice. This fairly justifies that PPP is more accurate model as the network degradation that are not taken into account for the hexagonal grid are indirectly incorporated. In addition, we observe that the performance gets worse with inter-user interference which is incurred by FD operation of the BS and the uplink UEs transmission. The loss incurred by the low-resolution ADC/DAC is about 2 dB when the CDF saturates.

Fig. 3 illustrates the uplink spectral efficiency versus the number of quantization bits (b) simulated with PPP tessellation network. We observe that the spectral efficiency increases with b and converges to a ceiling derived by Lemma 1 (24) while the rate is decreased by adopting low-resolution ADC/DAC (low b). We further observe the impact of the SI power how it degrades the spectral efficiency for 10 W and 40 W of SI power compared to the SI-free scenario.

Fig. 4 illustrates the downlink spectral efficiency versus the number of antennas at the BS simulated for PPP tessellation network. We observe that the rate increases with the number

TABLE II: System Parameters [6], [7], [11].

Parameter	Value
Bandwidth	20 MHz
Pathloss Exponent	3.5
Shadowing	5 dB
Downlink Transmit Power	40 W
Uplink Transmit Power	250 mW
SI Power	40 W
SI Channel Power	10 dB
Noise Spectral Density	-174 dBm/Hz
Number of antennas	100

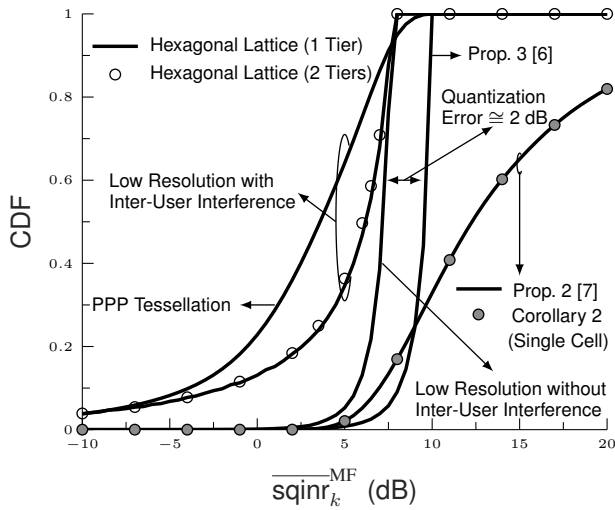


Fig. 2: Forward link performance results: Effects of full-duplexing, quantization error, and network cells shapes on the outage probability (CDF). With $\alpha_u = \alpha_d = 0.6$.

of quantization bits and antennas. When considering low-resolution and full-resolution data converters, the spectral efficiency converges to a fixed ceiling with an increased number of antennas, which agrees with Lemma 3 (29). Given that, the increase in the frequency reuse factor is often adopted to improve the cellular coverage; however, this increase is paid for by decreasing the rate in the network.

VII. CONCLUSION

In this work, we investigated the performance of FD massive MIMO cellular networks with low-resolution ADCs and DACs. Using matched filter precoding and combining at the BS with the AQNM model and with transmitters and receivers relying on channel hardening, we analyzed the SQINR CDF and spectral efficiency for reverse and forward links and for hexagonal and PPP networks. We further derived the asymptotic expressions and the power scaling laws. The results

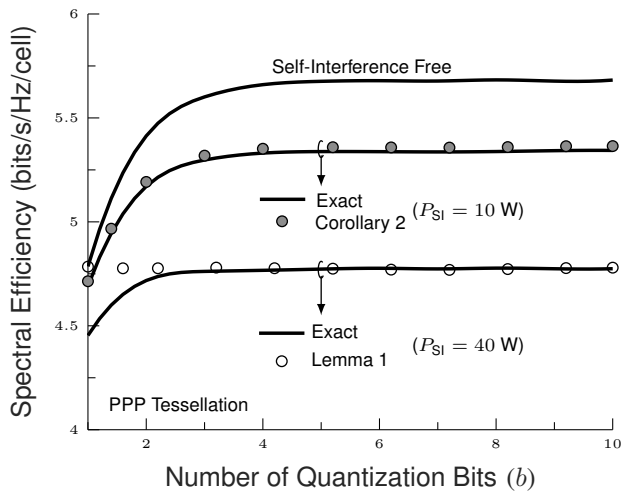


Fig. 3: Reverse link performance results: Impacts of the number of quantizations bit and the SI power on the spectral efficiency.

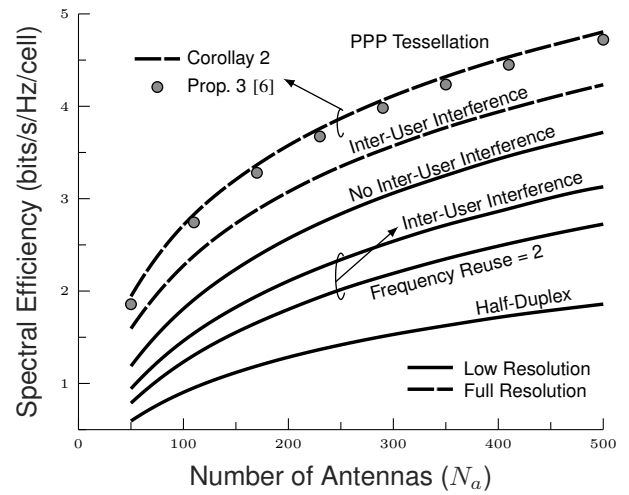


Fig. 4: Forward link performance results: Effects of the number antennas, duplexing modes, ADC/DAC resolution and frequency reuse factor on the spectral efficiency. With $\alpha_u = \alpha_d = 0.5$.

indicate that the quantization error and SI incur pronounced losses in the system performance; however, this loss can be compensated by using more antennas. Finally, this work shows the feasibility of FD with low-resolution ADCs and DACs in massive MIMO cellular networks.

REFERENCES

- [1] "The 5G Evolution: 3GPP Releases 16-17." [Online]. Available: <https://www.5gamerica.org/wp-content/uploads/2020/01/5G-Evolution-3GPP-R16-R17-FINAL.pdf>
- [2] E. Balti and B. L. Evans, "Hybrid beamforming design for wideband mmwave full-duplex systems," *ArXiv*, 2021. [Online]. Available: <https://arxiv.org/abs/2107.06166>
- [3] E. Balti and N. Mensi, "Zero-forcing max-power beamforming for hybrid mmwave full-duplex MIMO systems," in *International Conference on Advanced Systems and Emergent Technologies*, 2020, pp. 344–349.
- [4] R. W. Heath, N. González-Prelcic, S. Rangan, W. Roh, and A. M. Sayeed, "An overview of signal processing techniques for millimeter wave mimo systems," *IEEE Journal of Selected Topics in Signal Processing*, vol. 10, no. 3, pp. 436–453, 2016.
- [5] "5G: Study on New Radio (NR) access technology." [Online]. Available: https://www.etsi.org/deliver/etsi_tr/138900_138999/138912/15.00.00_60/tr_138912v150000p.pdf
- [6] G. George, A. Lozano, and M. Haenggi, "Massive mimo forward link analysis for cellular networks," *IEEE Transactions on Wireless Communications*, vol. 18, no. 6, p. 2964–2976, Jun 2019.
- [7] J. Dai, J. Liu, J. Wang, J. Zhao, C. Cheng, and J.-Y. Wang, "Achievable rates for full-duplex massive mimo systems with low-resolution adcs/dacs," *IEEE Access*, vol. 7, pp. 24 343–24 353, 2019.
- [8] W.-T. Li, Y.-C. Chiang, J.-H. Tsai, H.-Y. Yang, J.-H. Cheng, and T.-W. Huang, "60-ghz 5-bit phase shifter with integrated vga phase-error compensation," *IEEE Transactions on Microwave Theory and Techniques*, vol. 61, no. 3, pp. 1224–1235, 2013.
- [9] M. R. Akdeniz, Y. Liu, M. K. Samimi, S. Sun, S. Rangan, T. S. Rappaport, and E. Erkip, "Millimeter wave channel modeling and cellular capacity evaluation," *IEEE Journal on Selected Areas in Communications*, vol. 32, no. 6, pp. 1164–1179, 2014.
- [10] L. Fan, S. Jin, C.-K. Wen, and H. Zhang, "Uplink achievable rate for massive mimo systems with low-resolution adc," *IEEE Communications Letters*, vol. 19, no. 12, pp. 2186–2189, 2015.
- [11] T. D. Novlan and J. G. Andrews, "Analytical evaluation of uplink fractional frequency reuse," *IEEE Transactions on Communications*, vol. 61, no. 5, pp. 2098–2108, 2013.